Precipitation over the Interior East Antarctic Ice Sheet Related to Midlatitude Blocking-High Activity

ROBERT A. MASSOM,* MICHAEL J. POOK,+ JOSEFINO C. COMISO,# NEIL ADAMS,@ JOHN TURNER,& TOM LACHLAN-COPE,& AND TIMOTHY T. GIBSON**

*Antarctic Climate and Ecosystems Cooperative Research Centre, University of Tasmania, Hobart, Tasmania, Australia
+CSIRO Marine Research, Hobart, Tasmania, Australia
#Oceans and Ice Branch, NASA Goddard Space Flight Center, Greenbelt, Maryland
@Antarctic Climate and Ecosystems Cooperative Research Centre, University of Tasmania, and Australian Bureau of Meteorology, Hobart, Tasmania, Australia
&British Antarctic Survey, Cambridge, United Kingdom
**Antarctic Cooperative Research Centre, University of Tasmania, Hobart, Tasmania, Australia

(Manuscript received 4 February 2003, in final form 17 September 2003)

ABSTRACT

Intermittent atmospheric blocking-high activity in the South Tasman Sea is shown to play a key role in delivering substantial snowfall as far south as at least 75°S on the central East Antarctic Ice Sheet plateau. Typically, cyclones fail to penetrate this far (>1000 km) inland, and accumulation was thought to be dominated by clear-sky precipitation. In East Antarctica, the meridional cloud bands delivering the moisture originate from as far north as 35°–40°S, and appear to preferentially pass over the East Antarctic coast in a corridor from ~120° to 160°E. Comparison of surface observations, model, and satellite data suggests that a few such episodes contribute a significant proportion of the (low) mean annual accumulation of the central East Antarctic Ice Sheet (e.g., an estimated 44% at Dome C over 18 days in December 2001–January 2002). Blocking-high-related incursions also cause abrupt increases in the surface wind speed (snow redistribution) and air temperature; this has implications for the interpretation of ice core data. Blocking-high-related precipitation episodes can generally be detected over the ice sheet interior, via abrupt changes (of ~0.02–0.04) in polarization in 37- and 85-GHz SSM/I data, due to the relative stability of the surface and its ''background'' microwave signature and the relative lack of cloud cover overall. This is not the case in high-accumulation near-coastal regions such as Law Dome, where additional information is required. Ambiguities remain due to blowing snow and hoarfrost formation. Further research is necessary to examine the frequency of occurrence and variability of midlatitude blocking-high systems, their effect on precipitation in the Antarctic Ice Sheet interior, and the potential effect of global change.

1. Introduction

In this paper, we use case studies to demonstrate the episodic occurrence of significant precipitation events deep inland on the East Antarctic Ice Sheet, and the link between these events and intermittent blocking anticyclone activity at the midsouthern latitudes. Due to the sparsity of direct contemporary surface observations, this study relies on output from numerical weather prediction model analyses and satellite passive microwave data, with the latter providing an independent means of inferring snowfall events via their impact on ice sheet surface and therefore microwave properties. The importance of such events lies in the fact that the high plateau of Antarctica is the world's largest and driest desert (Schwerdtfeger 1984; Bromwich 1988). In the central East Antarctic Ice Sheet, the snow that falls each year is equivalent to only about 50 mm of rainfall (Bromwich 1988). Significant contrasts exist, however, between interior and coastal zones in terms of the mean annual accumulation of snow (Vaughan et al. 1999; Giovinetto and Bentley 1985), as shown in Fig. 1. Over central Antarctica, the 50-mm water-equivalent isopleth accords well with the estimate of mean annual precipitation there of around 50 mm of water equivalence, given that climatological wind speeds, and thus sublimation, are relatively low. In contrast, the accumulation rate on the eastern slopes of the near-coastal Law Dome, eastern Wilkes Land (~110 km east of Casey Base) exceeds 600-mm water equivalent per year. This meridional contrast results from orographic uplift of moisture-laden air masses prevailing from the east by the ice sheet as the air mass moves inland, and resultant moisture loss in the near-coastal zone in the form of snowfall (Bromwich 1988; Xie et al. 1989). Due to the higher ice sheet elevation in East Antarctica, cyclones penetrate

Corresponding author address: Dr. Robert Massom, Antarctic Climate and Ecosystems Cooperative Research Centre, c/o University of Tasmania, Private Bag 80, Hobart, Tasmania 7001, Australia.
E-mail: r.massom@utas.edu.au

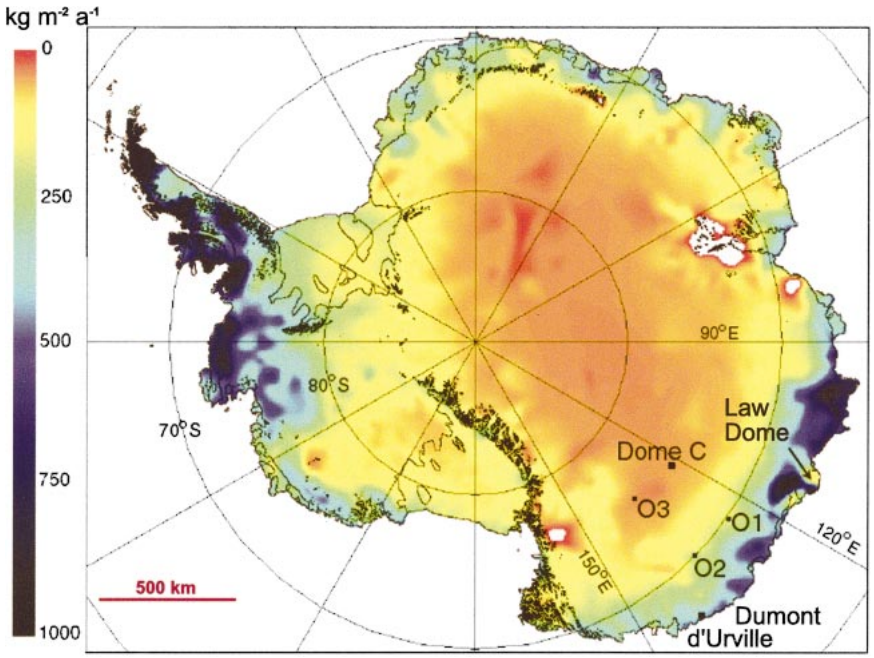

FIG. 1. A map of net surface mass balance precipitation minus evaporation per annum across Antarctica, computed by Vaughan et al. (1999) from an updated data compilation including analysis of atmospheric moisture transport into the region (e.g., Connolley and King 1993), combined with the earlier compilation of Giovinetto and Bentley (1985), which used glaciological data. Areas of interest are marked. Adapted from Vaughan et al. (1999).

this region much less frequently than they do interior West Antarctica (Bromwich 1988). For the continent as a whole, the estimated mean annual snow accumulation is equivalent to about 150 mm of water (Turner et al. 1999; van Lipzig et al. 2002).

Climatological studies (e.g., Carleton and Carpenter 1990; Murray and Simmonds 1991; Sinclair 1994) have suggested that cyclones and polar lows seldom if ever penetrate far inland onto the Antarctic Ice Sheet, with their impact being largely confined to the coastal margin. However, Pook and Cowled (1999) and Pook and Gibson (1999) have recently shown that major weather systems occasionally penetrate deep into the Antarctic continental interior. They further establish an association between the inland migration of lows and the incidence of intense anticyclonic blocking activity in the Tasman Sea (SW of New Zealand), which is a preferred region for blocking in the Southern Hemisphere (Pook 1995; Pook and Gibson 1999; Trenberth and Mo 1985; Wright 1974). Other regions of frequent blocking are the South Atlantic (Sinclair 1996) and SE Pacific Oceans (Marques and Rao 1999). A blocking anticyclone is defined as a tropospheric high pressure system that remains approximately stationary for $\geq$6 days in an area where zonal flow usually prevails, and the frequent passage of cyclones is the norm (Wright 1974). Autumn is the period of maximum blocking activity in the Tasman Sea/SW Pacific, with somewhat less activity in winter and spring and a definite summer minimum (Gibson 1995).

Pook and Cowled (1999) attribute the fact that deep inland incursions of heat and moisture have gone largely undetected to limitations in the observational network, the difficulty of resolving these features in numerical models and manual analyses, and the difficulty in distinguishing associated cloud signatures from the underlying ice surface due to similarities in their optical and thermal signatures (Turner and Row 1995). Furthermore, the elevation of the Antarctic Plateau, which rises from approximately 2 km close to the coast to over 4 km at its highest point, requires that synoptic and mesoscale systems moving inland have well-defined vertical structures in order to survive.

Pook and Cowled (1999) and Pook and Gibson (1999) cite an example of blocking from late July, 1994, in which a positive 500-hPa geopotential anomaly of at least 20 m (at 55°S) persisted in the southwest Pacific Ocean for approximately 1 week. We initially analyze satellite passive microwave data from this period to infer the occurrence of snow accumulation events related to blocking-high episodes, which are detected in meteorological data and satellite cloud pattern time series. The analysis is then extended to include similar cases from 1995 and 2001–02. Due to the large scales involved and the difficulty in accurately measuring accumulation on polar ice sheets in situ, research has evaluated satellite

microwave remote sensing as a means of gaining information on large-scale accumulation patterns (e.g., Fily and Benoist 1991; Zwally 1977; Zwally and Giovinetto 1995). Such studies rely on accurate and detailed knowledge of firn (upper ice sheet) properties through time and independent knowledge of the upper-snow-temperature profile with depth (Alley 1987; Comiso et al. 1982). This information is lacking here. As such, the estimation of absolute snow accumulation, which also needs to account for the net gains from snowfall, frost deposition, and drifting (Budd 1966), minus losses from sublimation and drifting (Warren 1996), is beyond the scope of this paper. We therefore use modeled operational analysis data to determine precipitation rates, and independently infer changes in ice sheet surface characteristics due to precipitation events associated with blocking highs from changes in satellite microwave emissions.

2. Data and methods

a. Study regions

This analysis concentrates on two contrasting regions of East Antarctica, namely, Dome C and Law Dome. These locations, marked in Fig. 1, were chosen as they underlay the cloud incursions but differ significantly in terms of their mean annual accumulation regimes. Centered at ~66.5°S, 113°E, Law Dome is a medium-sized, approximately circular ice sheet (diameter 200 km, elevation ~1400 m) adjoining the coastal edge of the main ice sheet. Projecting out into the prevailing easterly winds, it is an area of high annual accumulation (>1000 kg m^{-2} a^{-1}; Xie et al. 1989), particularly on its eastern flank and summit. Snow profile work carried out farther east by Goodwin et al. (1994) shows that the region also displays a strong gradient of decreasing accumulation with both increasing continentality and elevation. On the near-coastal slopes of Wilkes Land, extensive depth-hoar formation, which is indicative of low accumulation rates, is restricted to elevations above 2500 m. Depth hoar are large (one to several millimetres in diameter), cohesionless, coarse, faceted snow crystals which result from the presence of strong temperature gradients within the snowpack (Colbeck 1983).

Dome C, on the other hand, is much farther inland (at ~74.5°S, 124°E, ~1080 km from the coast) and high up on the Antarctic Plateau (elevation 3240 m). It is characterized by a much lower mean annual accumulation rate of ~30 kg m^{-2} a^{-1} (Palais et al. 1982). The mean annual air temperature is also very low (e.g., −51.5°C for 1994). Moreover, the mean wind speed drops off significantly from the coast to the continental interior at 120°E (Allison et al. 1993; Legresy and Remy 1997; Pettré et al. 1986; Wendler and Kodama 1984), and the region is characterized by minimal cloudiness.

Data were analyzed at a number of points along transects across the two study regions, and at three locations in the intervening region and to the east (O1–O3) as shown in Table 1. General surface conditions around O1 are described by Goodwin (1990, 1991) and Surdyk and Fily (1995). This region, which is at an elevation of ~2300 m, is characterized by fairly strong winds and a snow cover with a high surface density (420 kg m^{-3}) formed by wind packing, but with few strata in the upper few meters. The wind action also produces centimetre- to meter-scale surface roughness, with sastrugi and wind crusts being a dominant feature. Sastrugi are elongated wind-blown ridges of snow that are aligned in the prevailing wind direction, and may reach up to a meter in height.

TABLE 1. The names and locations of sites in this study.

Name	Lat, °S	Lon, °E
Law Dome		
LD1	66.73	113.62
LD2	67.85	112.50
LD3	67.85	113.62
Dome C		
DC1	73.46	122.62
DC2	73.46	123.75
DC3	74.58	122.62
DC4	74.58	123.75
DC5	75.70	122.62
DC6	75.70	123.75
Intervening sites		
O1	69.90	125.43
O2	70.08	135.11
O3	75.00	135.00

b. Detection and monitoring of weather systems

1) SATELLITE IMAGERY AND STUDY PERIODS

Incursions of relatively warm moist air were initially detected by manual analysis of cloud patterns in visible and thermal infrared data from the Defense Meteorological Satellite Program (DMSP) Operational Linescan System (OLS) and the National Oceanic and Atmospheric Administration (NOAA) Advanced Very High Resolution Radiometer (AVHRR) sensors. Visible [wavelength (λ) 0.40–1.10 μm] and thermal infrared [(λ) 10.0–13.4 μm] imagery from the OLS are at spatial resolutions of 0.55 (fine mode) and 2.7 km (smooth mode); the resolution of AVHRR data used (10.3–11.3 μm) is ~4 km.

Based upon this analysis, previous work by Pook and Cowled (1999) and Pook and Gibson (1999), and recent field observations at Dome C during the European Project for Ice Coring in Antarctica (EPICA; E. Wolff 2002, personal communication), three periods were chosen to illustrate the effect of large scale deep incursions of relatively warm, moist air, related to blocking events farther north. These are late July 1994, late July 1995, and mid-December 2001 to mid-January 2002. Data from April 1995 were also analyzed, but are not pre-

sented in detail here, as results are similar to those in July 1994.

As no contemporary observations of snowfall were available for the first two study periods, we used satellite passive microwave data to infer snowfall occurrences via their effect on the ice sheet surface microwave properties. Changes in the latter were detected using time series of brightness temperature (TB) data from the SSM/I onboard DMSP satellite *F11*. Individual SSM/I pixels were chosen to correspond to the locations in Table 1. Full-resolution orbital (''swath'') geolocated product data (Wentz 1991), collected at 19.35 (λ = 1.55), 37 (λ = 0.81), and 85.5 GHz (λ = 0.35 cm) [both vertical (*V*) and horizontal (*H*) polarization], were used in preference to daily averages to better resolve the rapid changes in surface properties related to snowfall. The spatial sampling interval of these swath data, which are mapped on the SSM/I polar stereographic grid using a simple linear interpolation technique, is 25 km at 19 and 37 GHz, and 12.5 km at 85 GHz. Overall, snow accumulation events are difficult to detect in TB time series alone. Work by Shuman and Alley (1993) and Mätzler et al. (1984), however, revealed that the *V*/*H* ratio is sensitive to short-term changes in ice sheet surface and near-surface properties, that is, it is related to snowfall. Following their work, *V*/*H* plots at 19, 37, and 85 GHz were produced. The use of a ratio minimizes the effect of changing physical temperatures of the radiating portion (i.e., the upper few meters, depending on frequency of radiation) of firn.

Working in Greenland, Shuman et al. (1993) found that abrupt changes in observed *V*/*H* resulted from changes in surface and near-surface microwave reflection rather than volume scattering from the upper few meters of snow (bulk). Reflection is a function of surface roughness (at the centimeter scale), snow density, incidence angle, and polarization (Shuman et al. 1993). At the 53.1° incidence angle of the SSM/I, which is close to the Brewster angle for snow, reflection of upwelling microwaves is negligible at *V* polarization (irrespective of other conditions), yet is significant for *H* polarization (Fung and Chen 1981; Remy and Minster 1991). Given the short time scale of our investigation (a few days in each case), we assume that internal reflection and volume-scattering effects remained relatively constant, with observed abrupt changes in the microwave signature resulting primarily from synoptic-scale changes in surface characteristics, primarily due to snowfall.

The following is brief background material to aid interpretation of the satellite observations. Abrupt changes in *V*/*H* depend upon the nature of the snowfall, the surface on which it falls, and the meteorological conditions at the time of precipitation. Relatively high *V*/*H* values occur when the snow–air interface is smooth with respect to the microwavelength, and/or the surface density is relatively high, causing preferential reflection of upwelling *H*-polarized microwave radiation relative to *V*-polarized microwave radiation (Fung and Chen 1981; Surdyk and Fily 1995). Due to the low net annual precipitation in the region (Fig. 1), high-density and smooth surface crusts are a common feature of inland Antarctica (Palais et al. 1982). Surface glazing occurs in summer by radiational effects, and in winter by the formation of regelation ice films on the snow surface due to kinetic heating of wind-driven saltating drift snow (Goodwin 1990). According to (Foster et al. 1984) and Surdyk and Fily (1995), crusts produce polarization differences by inducing strong density variations at interfaces.

The addition of a new, low-density snow layer on a higher-density surface can result in a significant decrease in *V*/*H*, with the magnitude depending on wind speed during and after snowfall. Surface density generally increases with wind speed (Male 1980). Under calm conditions, snowfall forms a soft surface layer with a bulk density as low as 200 kg m^{-3}, whereas windy conditions produce a fine-grained hard wind slab with a bulk density of 400 kg m^{-3} or more (Alley 1988). Winds can decrease the microwave reflection and increase *H* by their effect on the ice sheet small-scale surface roughness (Remy and Minster 1991). At SSM/I wavelengths, centimeter-scale microroughness features are likely the dominant factor affecting microwave emission rather than 0.1–1.0-m scale (vertical) sastrugi and snow dunes (Fung and Eom 1982; Ulaby et al. 1981). Moreover, sastrugi were unlikely to be a factor at Dome C at this time (Pettré et al. 1986), as they form under high winds with light or no snowfall, when the supply of snow is exceeded by the wind's ability to transport it (Alley 1987). An increase in surface roughness, and/or a decrease in surface density, results in multiple scattering, which decreases *H* reflection and increases *H* emission while slightly increasing *V* reflection and decreasing *V* emission (Remy and Minster 1991). A confusing factor can be the appearance of a surface hoarfrost layer, as discussed later. Hoarfrost forms from the deposition (sublimation) of ice crystals on the surface when the temperature of the surface is colder than the air above and the frost point of that air.

The passive microwave data are interpreted using contemporary meteorological observations and model data, and changes in surface conditions related to snowfall events inferred by a synergistic analysis of the combined dataset and, in the case of late 2001–02, direct observations at Dome C (E. Wolff 2002, personal communication). Surface observations are not available for 1994 and 1995.

2) METEOROLOGICAL DATA

Wind speed and direction and air temperature (T_{air}) data were used from the automatic weather stations (AWS) at Dome C [74.5°S, 123°E, elevation 3250 m MSL, World Meteorological Organization (WMO) site #89828] and Law Dome (66.73°S, 112.74°E, elevation

1366 m, WMO #89811). Midlatitude blocking-high episodes were detected both in upper-air observations from Macquaire Island (54.5°S, 158.93°E) and in modeled synoptic analyses of mean sea level pressure (MSLP) and wind fields. The latter were obtained from the National Centers for Environmental Prediction–National Center for Atmospheric Research (NCEP–NCAR) climate reanalysis dataset (Kalnay et al. 1996; Kistler et al. 2001). This is subsequently referred to as the NNR dataset. Airflows associated with the systems were detected crossing the Terre Adélie coast using meteorological data from the French station Dumont d'Urville (66.66°S, 140.02°E, WMO #89642, elevation 43 m).

As the magnitude of snowfall cannot be derived from the satellite data, daily precipitation totals (equivalent to precipitable water) for the points in Table 1 were computed from the European Centre for Medium-Range Weather Forecasts (ECMWF) operational model analysis. Because the assimilation scheme cannot analyze precipitation data, precipitation has been obtained from the forecast fields. Due to a spinup problem for precipitation in the first 12-h integration period (see Turner et al. 1999), data were taken from the 12–24-h period. The precipitation for each day was computed from two forecasts, for the 12–24-h period starting at 0000 UTC on the day and at 1200 UTC on the previous day. Recent studies show that the ECMWF Re-Analysis (ERA) precipitation over Antarctica compares favorably with estimates of accumulation from short firn cores (see Turner et al. 1999, their Fig. 6).

As ECMWF moisture data were only available for point locations, we also used regional maps of the precipitable water field that were obtained from the Antarctic version of the Australian Bureau of Meteorology's Local Area Prediction System (LAPS). The value obtained, which is a measure of the total column water content in millimeters, was derived by integrating the layer mean mixing ratio values from the surface to the model upper boundary. The Antarctic LAPS (ALAPS) system has a gridpoint resolution of 0.25° latitude by 0.5° longitude. The model is hydrostatic and employs a vertical sigma coordinate system with the lowest level at 0.9988 (~10 m off the ground) and the upper-sigma level at 0.05 (~20 km above the ground). For a full description of the LAPS model and polar modifications made in ALAPS, see Puri et al. (1998) and Adams (2001), respectively. Precipitable water fields from the ALAPS model have been used in this study because an investigation by Adams (2004) has shown that the precipitation fields from the high-resolution ALAPS datasets have provided useful precipitation forecasts over the high southern latitudes. MSLP and wind fields were also provided from the ALAPS output. Note that it was not possible to provide maps of aerologically determined precipitation minus evaporation ($P - E$) as the only soundings available in this part of Antarctica are at Casey (110.5°E) and Dumont d'Urville (140°E), Antarctica, both of which were on either side of the precipitation events analyzed here.

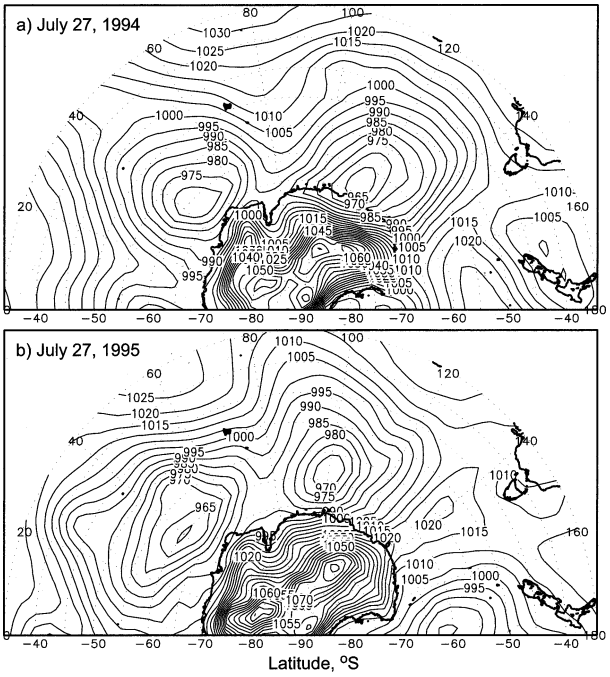

FIG. 2. NNR reanalysis charts of MSLP (hPa) at 0000 UTC for (a) 27 Jul 1994 and (b) 27 Jul 1995.

3. Results and discussion

a. Case study 1: July–August 1994

Analysis of OLS time series during 22–28 July 1994 (Pook and Cowled 1999) showed that while cyclonic vortices largely remained to the north of the Antarctic coast, cloud bands from these systems moved inland at regular intervals. The NNR MSLP chart for 27 July 1994 shows a well-defined anticyclone to the south of New Zealand (Fig. 2a). On this day, several vortices were observed to move across the East Antarctic coast and penetrate well inland (Pook and Cowled 1999). Prior to this, there was a deep inflow of moisture across the Adélie Land region. Figure 3 shows a frontal cloud band extending southward from at least 45°S across the Antarctic coast in the vicinity of Dumont d'Urville, on (a) 25 July and (b) 27 July. The relative absence of cloud to the east is consistent with the identification of a ''blocking'' high pressure system to the southwest of New Zealand by Pook and Gibson (1999) and Pook and Cowled (1999). Time series of atmospheric temperature and dewpoint from twice-daily radiosonde records at Dumont d'Urville confirm that the temperature rose steadily during the latter part of July 1994 (Fig. 4). The dewpoint depression (temperature dewpoint) remained below 2°C at 850 hPa from 25 to 28 July, suggesting the sustained advection of maritime air at this level. Figure 4 also demonstrates that the geopotential height

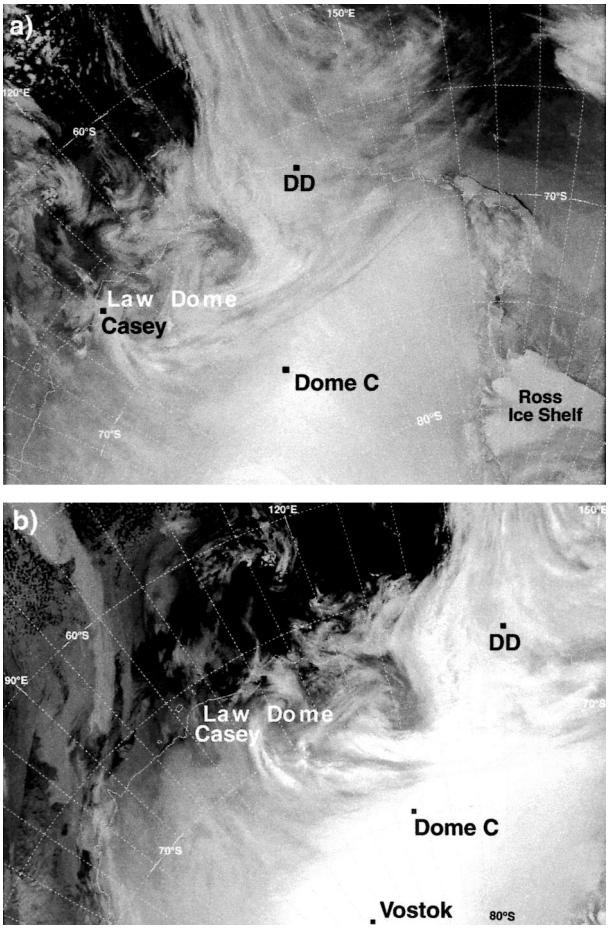

FIG. 3. A sequence of DMSP OLS images of cyclonic vortices over the East Antarctic Ice Sheet at approximately (a) 2300 UTC 26 Jul 1994, and (b) 0140 UTC 27 Jul 1994. DD: Dumont d'Urville. [From Pook and Cowled (1999) and Pook and Gibson (1999).]

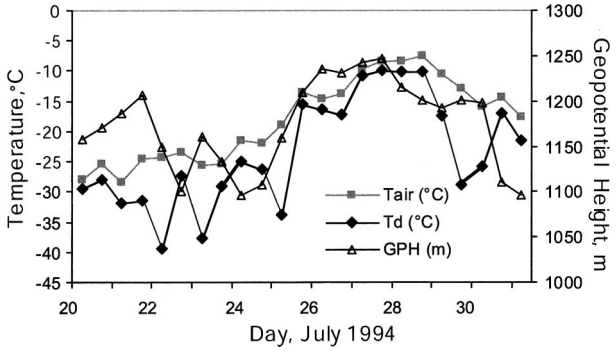

FIG. 4. Time series of air temperature (T), dewpoint (T_d), and geopotential height (GPH, at 850 hPa), Dumont d'Urville base, 20–31 Jul 1994.

of the 850-hPa surface rose by approximately 150 m during this period, confirming that the blocking ridge strengthened near the Adélie Land coast. At Macquarie Island, to the northeast of Dumont d'Urville, the ridge reached peak intensity at 850 hPa on 27 July (not shown).

1) DOME C AND "OTHER" SITES

Contemporary observations from the Dome C AWS confirm that the easternmost of these vortices passed deep inland and close to this station on 25 July 1994. This caused a rapid increase in wind speed from ~2 m s^{-1} at 0000 UTC on 27 July to 7.1 m s^{-1} at 1200 UTC, before decreasing to 0.0 m s^{-1} 12 h later (Fig. 5a). While this change is not great by normal coastal Antarctic standards, it is significant for Dome C, where very calm conditions prevail (Allison et al. 1993); the mean wind speed for July 1994 was 2.6 ± 2.5 m s^{-1} from a mean direction of 183° (Pook and Cowled 1999). Over the incursion period, the wind direction changed from easterly to northerly, then back to easterly. Large air temperature changes also occurred (Fig. 5a), with a rapid increase of ~30°C (from ~−74° to −42°C) on July 27, followed by a decrease of ~25°C over the subsequent 2–3 days.

That the cloud incursion led to light-to-moderate snowfall is supported by ECMWF daily precipitation totals shown in Fig. 5b, which peak at ~1.72 mm day^{-1} on 28 July. Analysis of SSM/I V/H time series provides further insight into the effect on ice sheet surface conditions. As shown in Fig. 5c, abrupt changes in V/H at Dome C correspond to the occurrence of snowfall and associated changes in T_{air} and wind speed. To the north (at site DC1) and as far south as DC4, large V/H decreases of 0.04–0.05 occur from 27 to 29 July (marked A–B in Fig. 5c), with the effect of new snowfall on surface conditions and therefore microwave signature increasing with increasing microwave frequency. This is consistent with other studies (e.g., Mätzler et al. 1984; Shuman and Alley 1993). The effect is less apparent at the two southernmost sites (e.g., DC6), apart from a temporary perturbation at 37 GHz (marked U in Fig. 5d). This suggests that the incursion had a significant effect on the ice sheet surface as far south as almost 75°S, although it was beginning to dissipate at this latitude. Indeed, snowfall at DC5–6 was equivalent to <0.5 mm day^{-1} precipitable water on 28 July, compared to ~1.7 mm day^{-1} at DC1–4. Data from site O3 to the east (at 75°S, 135°E) are presented in Fig. 6c. The decrease in V/H, marked U', is similar to that at Dome C (Fig. 5c), showing that the incursion episode affected a large area of the interior ice sheet. The signature is, however, obscured at site O1 (not shown), which is closer to the coast, while missing data preclude a detailed analysis at O2.

While atmospheric effects are negligible at 19 and 37 GHz (Sherjal and Fily 1994), 85-GHz data contain a signal both from the cloud incursion itself and from the surface e.g., from 25 to 31 July (point A to point B in Fig. 5c). At this frequency, ice and precipitation particles in the atmosphere have dimensions equivalent to

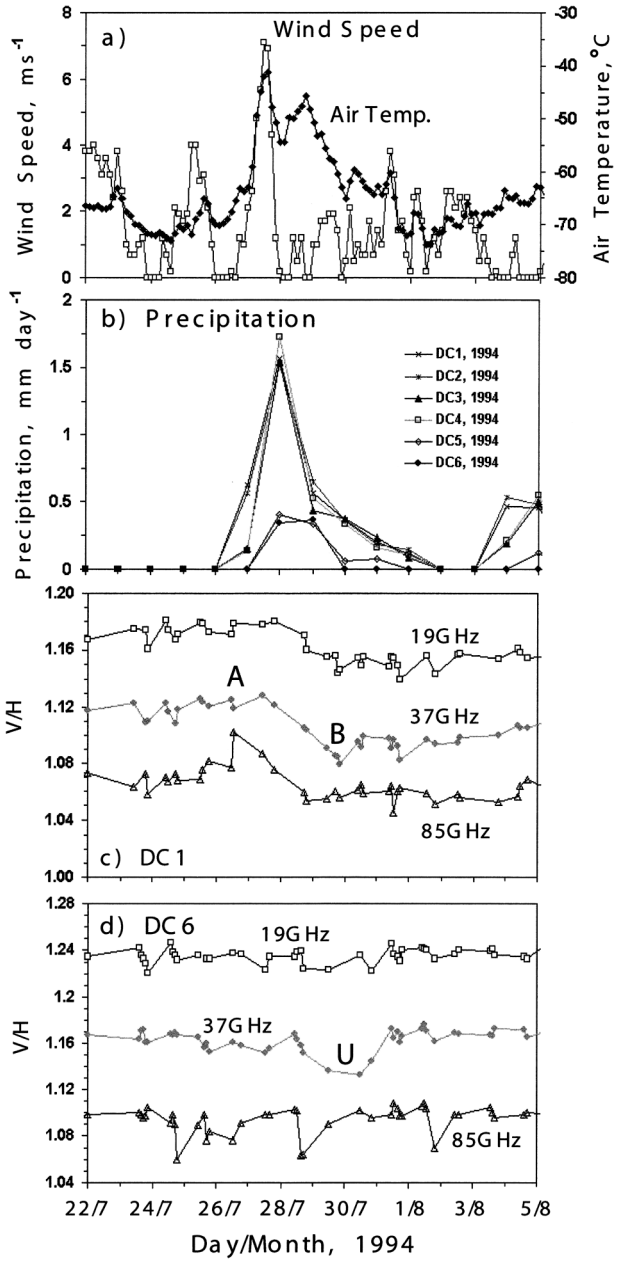

FIG. 5. (a) Time series of near-surface wind speed and air temperature from the Dome C AWS; (b) ECMWF 24-h accumulated precipitation totals for DC1–DC6; and *V*/*H* time series of SSM/I 19-, 37-, and 85-GHz data at (c) DC1 and (d) DC6: 22 Jul–5 Aug 1994.

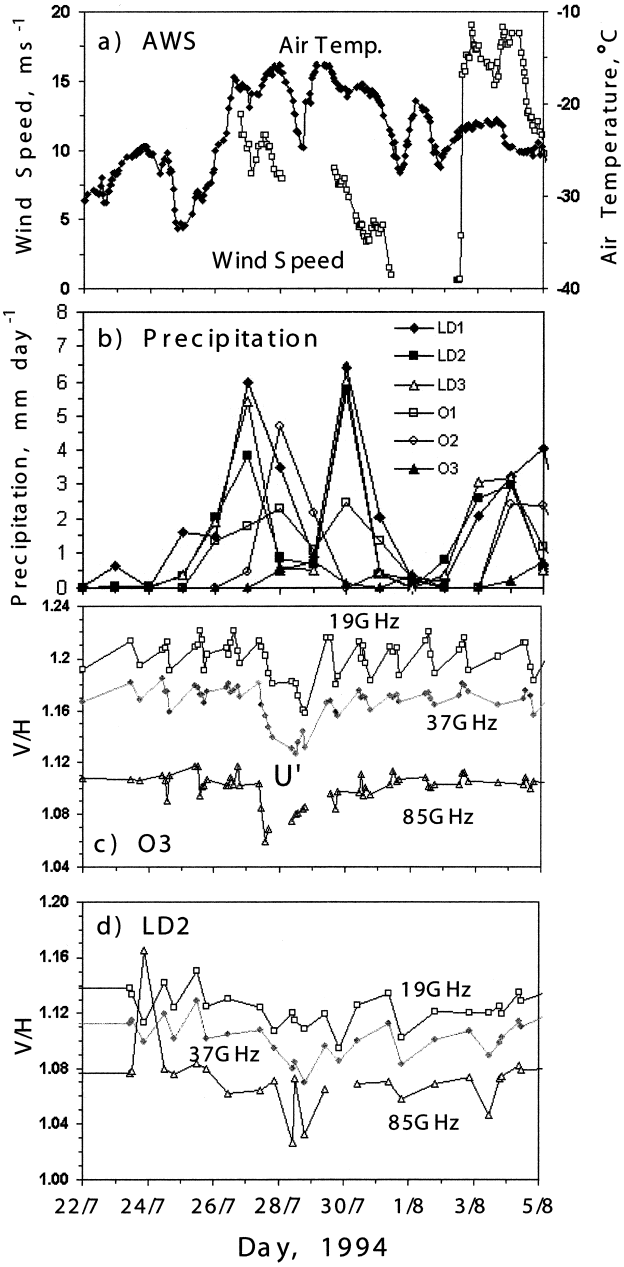

FIG. 6. (a) Time series of near-surface wind speed and air temperature from the Law Dome AWS; (b) ECMWF 24-h accumulated precipitation totals for LD1–LD3 and O1–O3; and *V*/*H* time series of SSM/I 19-, 37-, and 85-GHz data at (c) O3 and (d) L2: 22 Jul–5 Aug 1994.

the wavelength of the radiation ($\lambda = 0.35$ cm) and cause scattering (Mohr and Zipser 1996; St. Germain 1994). Higher-frequency data are included as atmospheric effects were minimal at this time once the cloud systems dissipated.

2) LAW DOME

Similar contemporary behavior is noted at Law Dome (Fig. 6d), with large increases in T_{air} and wind speed (Fig. 6a) accompanying periods of significant snowfall (Fig. 6b), with two peaks of ~6 mm day^{-1} in the ECMWF computation. Contemporary signals in the *V*/*H* time series are, however, much less clear than those at the inland sites. Of the three Law Dome sites, a relatively clear signal is only apparent at site LD2 (Fig. 6d), where it increased with increasing frequency to attain a maximum decrease of ~0.05 at 85 GHz between 27 and 28 July. High temporal variability in *V*/*H* profiles

at LD1 (on the summit) and LD3 (not shown) masks the effect of the incursion event on surface and near-surface properties. This variability is associated with the more regular, synoptic incursion of cyclones across this near-coastal zone, and the variable surface conditions and resultant high accumulation rates, as shown in Fig. 1. As such, the episode in late July 1994 is largely indistinguishable from the ''background'' signature in the *V*/*H* time series.

b. Case study 2: Late July 1995

Similar cloud incursion patterns occurred over a number of other periods, as detected in OLS and AVHRR data. A midlatitude blocking episode in late July 1995, for example, forced a cloud vortex deep inland in virtually the same region as the previous year. The MSLP chart for 27 July shows a well-defined ridge running north–south along 140°E to a very strong high-Plateau anticyclone, coupled with a deep low pressure center at ~110°W (Fig. 2b). This configuration had the effect of blocking the low moving in from the west, and advecting moist airstreams into the Antarctic continental interior. The frontal cloud band passed over the coast just to the east of Dumont d'Urville, at approximately the same location as in July 1994. At Macquarie Island, the geopotential height at 500 hPa rose to more than 5500 m on 30 July, and remained above this value until 3 August; the mean in August was 5317 m. Mean sea level pressure at Macquarie Island, Dumont D'Urville, and on the Australian Research Vessel R/V *Aurora Australis* (~100 km north of Dumont d'Urville) exceeded 1000 hPa over a period of approximately 1 week as the ridge extended southwestward across Adélie Land. At 0000 UTC on 6 August, the MSLP at Dumont d'Urville peaked at 1027.7 hPa, the highest barometric pressure ever recorded there in August.

1) DOME C

The effect on the *V*/*H* time series across Dome C is shown in Figs. 7c,d. A significant rise in *V*/*H* occurred across the region and at 19–85 GHz over a 4–5-day period (26–30 July, marked D–E), with the magnitude again decreasing with distance from the coast. This coincided a wind speed increase from approximately 0 to ~10 m s^{-1} over the same period, together with a decrease in pressure (from 670 to 650 hPa) and a large rise in T_{air} (from −60° to −40°C; Fig. 7a). Significant snowfall occurred, with peaks of ~0.71 mm day^{-1} on 27 July and 0.97–1.11 mm day^{-1} on 1–2 August at DC3–6 (Fig. 7b). In contrast to July 1994, the signature was now stronger at 19 than at 37 GHz, apart from at DC6. The subsequent decrease in *V*/*H*, marked E–F, coincided with a drop in wind speed (back to 0–2 m s^{-1}), a rebound in pressure (to 670 hPa), and T_{air} fluctuating between −45° and −57°C after a 20°C decrease on 30 July (at point E). This was followed by a *V*/*H* increase from 2 August (F–G), corresponding to an increase in temperature. This case again illustrates the complexity of processes affecting the microwave signature of the inland ice sheet surface, and the difficulty of interpreting satellite microwave data in isolation.

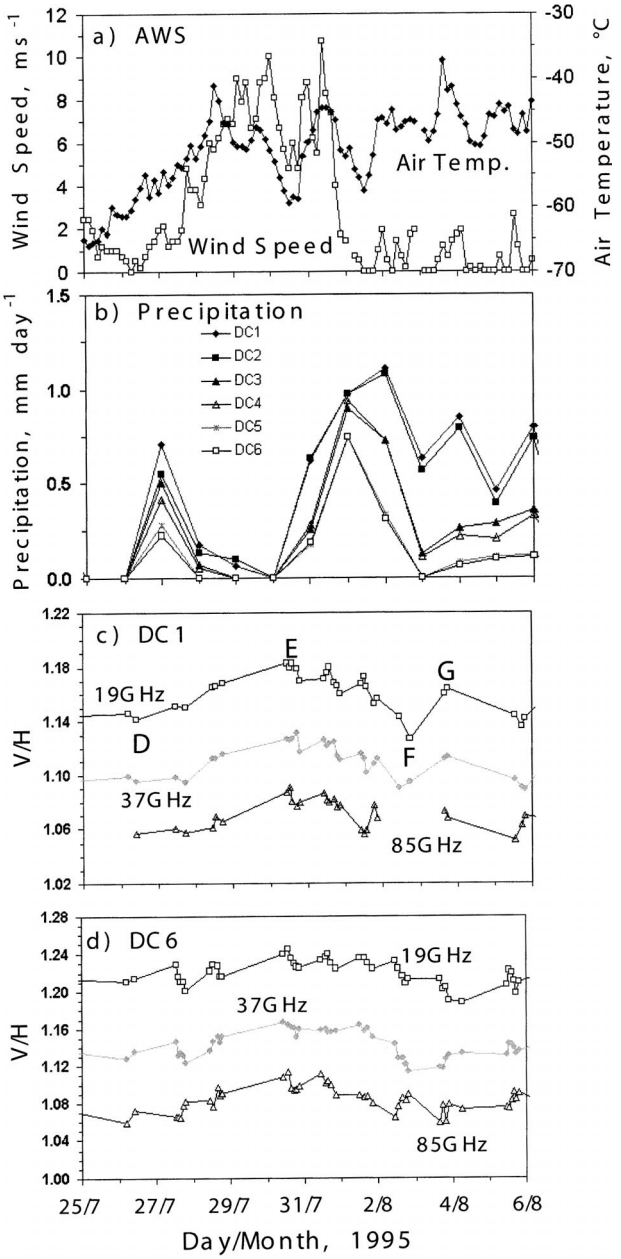

FIG. 7. (a) Time series of near-surface wind speed and air temperature from the Dome C AWS; (b) ECMWF 24-h accumulated precipitation totals for DC1–DC6; and *V*/*H* time series of SSM/I 19-, 37-, and 85-GHz data at (c) DC1 and (d) DC6: 25 Jul–6 Aug 1995.

2) LAW DOME AND ''OTHER'' SITES

Contemporary precipitation rates and V/H profiles at Law Dome site LD3 and ''other'' site O3 are shown in

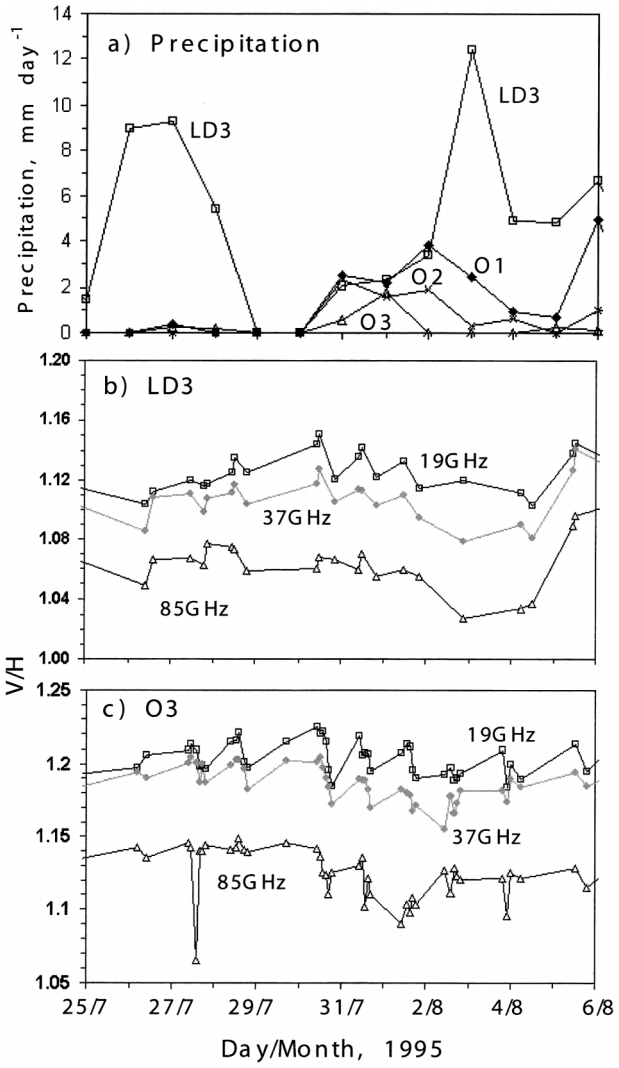

FIG. 8. Time series of (a) ECMWF 24-h accumulated precipitation totals for LD3 and O1–O3; and *V*/*H* time series of SSM/I 19-, 37-, and 85-GHz data at (b) LD3 and (c) O3: 25 Jul–6 Aug 1995.

Fig. 8. Again, an extensive area of the ice sheet was affected, with the overall *V*/*H* pattern at Dome C (Fig. 7) being apparent at both LD3 and LD2 (not shown) and the intervening other sites. Timings differ, with the peaks and troughs occurring slightly earlier to the north and east (consistent with the timing of the passage of the cloud band). Again, the signature was strongest at 85 GHz. The *V*/*H* signatures dropped significantly at O1 and O2 as cloud crossed the area on 30–31 July, while the signal at O3 to the southeast exhibits high diurnal variability (Fig. 8b). A similar pattern occurred at O3 from July to August 1994 (Fig. 6c). Precipitation at Law Dome was again substantially higher (Fig. 8a), peaking at 9.32 mm day^{-1} on 27 July compared to 0.40 mm day^{-1} at O1, and 12.39 mm day^{-1} on 3 August compared to 3.84 mm day^{-1} on 2 August. This again shows that snowfall occurred over a wide area.

Over Law Dome, the study period falls within the annual period of maximum snowfall (June–August) (Goodwin 1991). In July–August, icy surface layers appear not to be a factor in the region. As a result, the incursion event, while it delivered substantial snowfall to Law Dome (Fig. 6b), is difficult to identify in the SSM/I *V*/*H* signatures alone (Fig. 5d). The Law Dome *V*/*H* record is characterized by a high degree of temporal variability at this time, making it difficult to unambiguously distinguish unique signatures associated with the incursion from ''background noise'' (particularly at 19 GHz). This variability in the microwave signature is often diurnal, and may be related to the pattern of katabatic winds draining seaward from the continent.

c. Case study 3: December 2001–January 2002

The third case study, from December 2001 to January 2002, illustrates the complexity of atmospheric forcing and its effect on surface properties and the microwave signature of the interior ice sheet plateau. Strong signals were noted in the passive microwave record at this time. Figure 9a shows *V*/*H* profiles for the period 1 December 2001 to 20 January 2002 at DC3. A large decrease in polarization occurred on 20 December, after relative stability in the signature throughout November and most of December. A similar pattern occurred at O3 (not shown). In this case, it was caused not by snowfall but by extensive surface hoarfrost formation (E. Wolff 2002, personal communication). Formed under clear calm conditions (Lang et al. 1984), hoarfrost reduces the near-surface density and increases surface roughness at the approximate scale of the wavelength of the emitted radiation (Shuman and Alley 1993; Shuman et al. 1993). In this case, the hoarfrost crystals had a height and surface roughness scale of ~5 mm. Together, these effects would reduce *H* reflection and increase *H* emission, while slightly increasing the *V* reflection and decreasing the *V* emission, thereby decreasing the *V*/*H* ratio (Fung and Chen 1981).

The abrupt upturn in *V*/*H* on 28 December, however, coincided with a major inland incursion of cloud (Fig. 10) and moisture (precipitable water), as shown in ALAPS model output (Fig. 11), together with an associated wind speed increase and subsequent snowfall. The second scenario involved a strongly meridional cloud pattern in the vicinity of ~130°–140°E in the AVHRR mosaic of 29 December 2001 (Fig. 10). This pattern bears a strong resemblance to the patterns initially seen in July 1994 (Fig. 3), although NNR model output (Fig. 12) suggests that the advection of moisture-bearing air masses was in 2001 associated with a series of slowly moving cyclones to the north of the Antarctic coast. The interaction of these lows (marked L1 and L2 in Fig. 12), together with a narrow ridge of high pressure to the east and between southeastern Australia and Dumont d'Urville, set up a persistent airflow from the N–NE. In other words, the main mechanism for steering

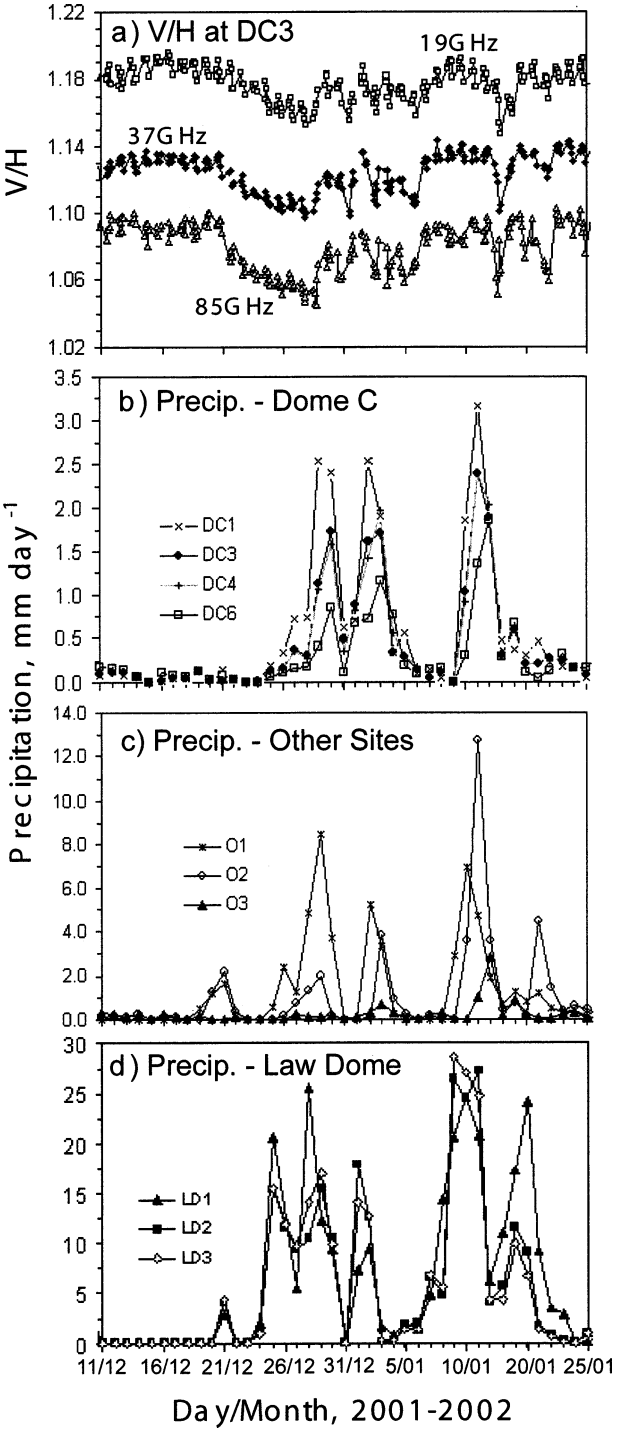

FIG. 9. (a) *V*/*H* time series of SSM/I 19-, 37-, and 85-GHz data at DC3; and ECMWF 24-h accumulated precipitation totals for (b) DC1, DC3, DC4, and DC6, (c) 01–03, and (d) LD1–LD3: 11 Dec 2001–20 Jan 2002.

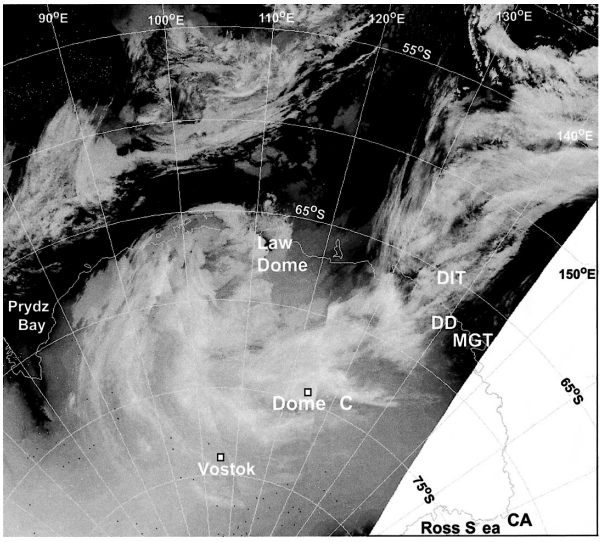

FIG. 10. A mosaic of AVHRR images (resolution 4 km) of East Antarctica, 0135 UTC, 29 Dec 2001, showing a blocking-high-related cloud band extending from low latitudes across to the interior ice sheet. DIT: Dibble Iceberg Tongue, DD: Dumont d'Urville, MGT: Mertz Glacier Tongue, and CA: Cape Adare. (Image courtesy of Australian Bureau of Meteorology and Australian Antarctic Division.)

moisture deep inland and onto the ice sheet plateau to beyond 80°S was not in this case a classic blocking high in the South Tasman Sea, yet the effect was much the same. Originating far to the north, this cloud band transported considerable moisture to the continental interior, as confirmed in the ALAPS precipitable water output (Fig. 11). Relative humidity values just on the coast near 130°E at 2300 UTC 27 December 2001 were >85% and indicative of cloud. By 2300 UTC on 28 December 2001, a band of very high (>98%) humidity crossed the coast at 125°E. By 2300 UTC on 29 December, the very moist band had moved westward to around 115°E, although a moist area of midlevel air extended inland, centered near 72°S, 118°E with a relative humidity of >85%. Note the low humidities elsewhere on the Antarctic continent at this time. Again, while the magnitude of resultant snowfall at and beyond ~75°S was relatively small by Law Dome standards, it was significant for Dome C, where clear-sky precipitation of diamond dust has been thought to predominate.

Snowfall occurred at Dome C for a few hours around 1600 UTC on 29 December, with an estimated accumulation of 3 mm (E. Wolff 2002, personal communication); this amount is similar to the ECMWF model estimate at this time (Fig. 9b). The increase in wind speed also affected the *V*/*H* signature by causing light drift that destroyed the surface hoarfrost cover, smoothed the microscale surface roughness and increased the near-surface snow density (E. Wolff 2002, personal communication). The surface now reflected more *H* radiation relative to *V* radiation (Shuman and Alley 1993), leading to a rapid increase in *V*/*H*. In this case, the change in surface properties was also detected in the 19-GHz signature. A similar pattern is observed ~200 km to the east at O3, but not at the other sites.

A second major snowfall peak at Dome C and other sites 3–4 days later (on 3 January) was also associated

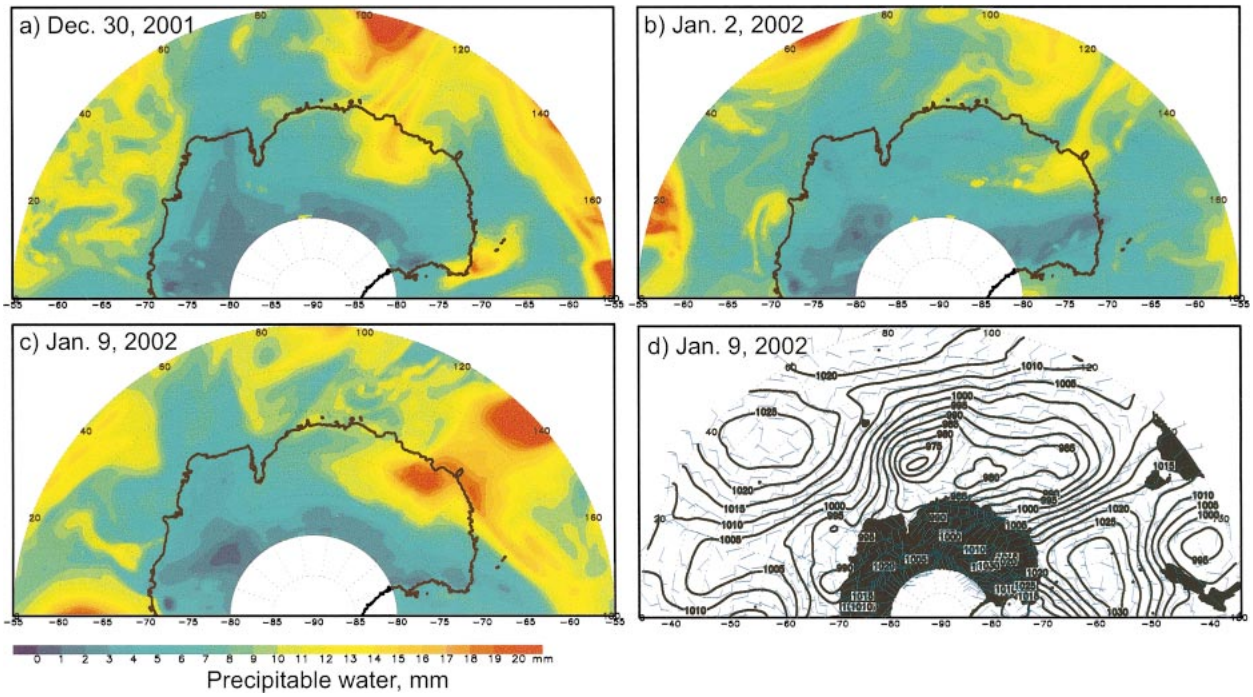

FIG. 11. Maps of ALAPS total precipitable water integrated through the column (in mm) for (a) 30 Dec 2001, (b) 2, (c) 9 Jan 2002, and (d) ALAPS MSLP (hPa) and 0.9988 sigma level winds (kt) for 9 Jan 2002, all at 2300 UTC.

with a meridional band of cloud crossing the coast in the region of ~130°–140°E, resolved in Fig. 11b and originating from latitudes lower than 50°S. The classic blocking-high effect returned on 9 January, as shown in ALAPS MSLP charts in Fig. 11d, with the meridional transport maritime air masses on its western flank (ALAPS rather than NNR output were used here or consistency with Figs. 11a–c). The meridional cloud band again emanated far to the north and crossed the coast in the vicinity of 120°–150°E. This incursion event alone contributed an estimated ~16% (or ~8.06 mm day^{-1}) of the mean annual snowfall at Dome C over only a 6-day period (9–14 January 2002). The magnitude of the moisture incursion can be seen in the ALAPS precipitable water map in Fig. 11c. Coincident decreases in *V*/*H* were related to light-to-moderate snowfall events peaking on 2–3 and 10 January 2002.

Substantial snowfalls, of up to ~3–13 mm day^{-1}, were also observed at sites O1–O3. The pattern described above was largely mirrored at Law Dome (Fig. 9d), with snowfall an order of magnitude greater than at Dome C. Peak snowfall events align in all cases. However, these episodes are again difficult to distinguish in the *V*/*H* time series from the coastal Law Dome sites (not shown), which are complex and exhibit a high degree of variability on semidiurnal to synoptic scales.

4. Conclusions

This paper has demonstrated that intermittent blocking-anticyclone events in the South Tasman Sea (centered on ~55°S, 140°–150°E) can cause significant precipitation events on the East Antarctic Ice Sheet by conveying warm and moist air masses deep into the continental interior, thousands of kilometers to the southwest. In each of the case studies presented, modeled precipitation events are largely consistent with cloud and synoptic analyses and also snowfall events independently inferred from DMSP SSM/I satellite data. Earlier work (e.g., Bromwich 1988) suggested that while snowfall occurs from clouds and is generated by orographic uplift and associated adiabatic cooling below 3000-m elevation, ''diamond dust'' (ice crystal) precipitation from clear skies is the dominant mechanism above this level (i.e., high on the East Antarctic plateau). Blocking-related episodes such as those described here lead to intermittent but significant snowfall over a wide sector of the high East Antarctic Ice Sheet desert plateau (>1000 km from the coast) and as far south as Dome C (~74.5°S) at least. Similar processes have been observed in Dronning Maud Land by Noone et al. (1999), and in the region of Dome Fuji (~77.32°S, 39.7°E) by Enomoto et al. (1998) and Hirasawa et al. (2000). In Wilkes Land and Terre Adélie, meridional cloud bands delivering the moisture originate from as far north as 35°–40°S, and appear to preferentially pass over the East Antarctic coast in a corridor from ~120° to 160°E. Slowly moving cyclones offshore can also have this effect in the absence of major blocking, when they align in a certain fashion. Diamond dust may still be an important process of inland accumulation at other times (E. Wolff 2002, personal communication).

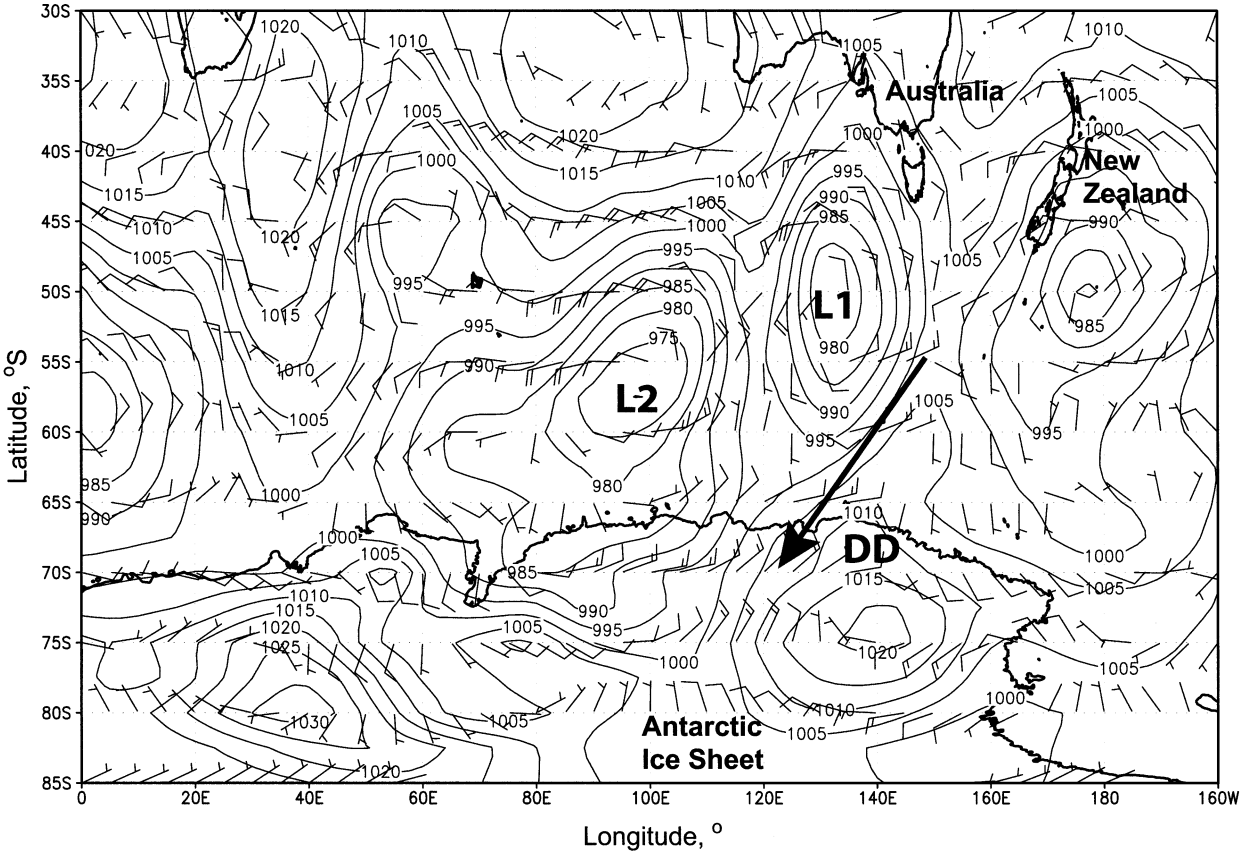

FIG. 12. Map (Mercator projection) of NNR MSLP (hPa) and 0.991 (~75 m) sigma level winds (m s^{-1}) over Antarctica and the Indian and western Pacific Ocean sectors for 28 Dec 2001 (0000 UTC). DD: Dumont d'Urville. The arrow denotes the maritime airmass incursion.

Importantly, it appears that a few such blocking-high episodes contribute a significant proportion of the (low) mean annual accumulation of inland desert regions of the East Antarctic Ice Sheet such as Dome C. They also contribute a lower, though still significant, proportion of snow to high-accumulation coastal regions such as Law Dome. The July 1994 blocking-high-related cloud incursion delivered an estimated ~6%, or ~3 mm day^{-1}, of the total mean annual accumulation of 50-mm water equivalent at Dome C (DC4) over only a 6-day period. The equivalent total over a 10-day period in July 1995 was >13% (at DC1). Moreover, the two deep incursions in late December 2001–mid January 2002 delivered an estimated ~27% and ~17% of the total mean annual accumulation over 11- and 7-day periods, respectively. Important deflation and evaporation effects (Smith et al. 1998) remain undetermined in this analysis.

These incursion episodes not only contribute significant snowfall; they also have a first-order impact on ice sheet surface and near-surface properties by abruptly increasing surface wind speed and T_{air} in an environment characterized by prevailing low temperatures and calm conditions. The austral summer of 2001/02 was characterized by persistent longwave amplified, or blocking, activity, causing warm moist air masses to penetrate high up onto the Antarctic plateau (Turner et al., 2002). On 11 January 2002, Vostok (78.5°S, 106.9°E, elevation 3488 m) experienced a temperature of −16.5°C, close to the record high for the station of −13.3°C (on 6 January 1974). Similarly, South Pole station had a maximum temperature of −18.1°C and a peak wind speed of ~16.5 m s^{-1} on 11 January 2002. Please see Sinclair (1981) for a description of earlier events. Incursion episodes also have implications for the transport and deposition of aerosols, pollutants and chemical constituents, and sublimation rates. Moreover, they have a dramatic though ephemeral impact on the sea ice cover surrounding Antarctica and its snow cover in winter, leading to significant episodic melt even in winter (Massom et al. 1997, 1998).

Snowfall occurrence can generally be detected in the relatively quiescent conditions and low-accumulation zone of the central East Antarctic Ice Sheet plateau via abrupt polarization changes, of ~0.02–0.04, in SSM/I 37- and 85-GHz data, with modeled moisture fluxes providing estimates of the magnitude of precipitation. Comparison with limited in situ observations in late 2001–early 2002 from Dome C suggests that the ECMWF estimates of daily precipitation totals are reasonably accurate. More work is required to examine this.

In high-accumulation near-coastal regions such as Law Dome, however, the similar unambiguous detection of snowfall episodes in the passive microwave record is limited. Here, the polarization signature of blocking-high-related snowfall tends to be swamped by high temporal variability in snowfall and wind speed (aeolian redistribution) associated with the synoptic-scale passage of cyclones.

Uncertainties remain in the interpretation of satellite passive microwave data over the ice sheet. For example, snow blowing across the surface during ''incursion episodes'' may itself impact the passive microwave signature at higher frequencies ($\geq$37 GHz), and may contribute to the close correspondence noted between changes in wind speed and the V/H signature. Another potential source of ambiguity is periodic surface hoarfrost accumulation, which can cause abrupt changes in V/H of a similar magnitude. In the absence of in situ observations and AWS data, different causal effects can be distinguished by analysis of cloud patterns in satellite visible/thermal IR imagery, with hoarfrost less likely during cloud incursions, which also imply an increase in surface wind speed (destructive to hoarfrost). More in situ observations are required to both test model output and quantify the effects of ice sheet surface variability on satellite microwave polarization signatures.

Modeling studies by Budd and Simmonds (1991) suggest that, over the next 100 yr, the most important impact of changes in Antarctic Ice Sheet mass balance on global sea level will result from increased precipitation minus evaporation ($P - E$) over grounded ice. The relative importance of blocking-high-related precipitation over the interior ice sheet desert is unknown under such a scenario. Clearly, developing an improved understanding of the present-day role of midlatitude blocking highs in poleward moisture transport is important if we are to better understand the response of the Antarctic Ice Sheet to predicted global warming (Bromwich et al., 1998). Better understanding of moisture sources and pathways related to blocking-high episodes, and their variability in time, is also required to improve the interpretation of climate-related Antarctic ice core data (Delaygue et al. 2000; McMorrow et al. 2001; Noone and Simmonds 1998). Questions also remain about the possible complex interplay between midlatitude blocking-high patterns and major oscillatory patterns in high southern latitude ocean–atmosphere processes—for example, the semiannual oscillation, the Antarctic Circumpolar Wave, (Reid and Budd 1999; White and Peterson 1996), and the El Niño–Southern Oscillation (ENSO). The interannual variability of Antarctic precipitation has been linked to ENSO by Cullather et al. (1996), and enhanced blocking activity related to ENSO by Renwick (1998).

Absolute estimates of ice sheet accumulation are currently not possible using the passive microwave data alone. The Geoscience Laser Altimeter System (GLAS) launched onboard the Ice, Cold, and land Elevation Satellite (ICESat) in January 2003 (Zwally et al. 2002) will potentially enable estimates to be made of the magnitude of accumulation resulting from individual blocking-high episodes, although such sensors are affected by cloud cover. Future work may benefit from the new generation of AWSs deployed in East Antarctica; these instruments include sonic surface-height detectors to record individual snow-accumulation events. Bromwich (1990) further suggests that improvements in the climatological atmospheric database should make possible more reliable and accurate estimates of Antarctic precipitation variations. In terms of estimating accumulation rates, a problem remains in determining the relative magnitudes of precipitation versus aeolian redistribution and sublimation, the latter being major factors in Antarctica.

Further research is necessary, and is taking place, to examine the frequency of midlatitude blocking highs, and their seasonal to interannual variability. This work will include the improved detection of meridional cloud incursions over the inland Antarctic plateau using the satellite passive microwave data record. It will benefit from improved data from the new Advanced Microwave Scanning Radiometer (AMSR) sensors on board the National Aerorautics and Space Administration (NASA) Earth Observing System *Aqua* satellite (launched May 2002) and the Japanese *Advanced Earth Observing Satellite II* (*ADEOS II*) (launched December 2002), and improved atmospheric model data.

Acknowledgments. The authors are very grateful to numerous people who contributed to this study. SSM/I swath data were obtained from Dr. Frank Wentz (Remote Sensing Systems Inc.). NOAA AVHRR imagery collected at Casey Base were supplied by the Australian Bureau of Meteorology (BoM) and Australian Antarctic Division (AAD); sincere thanks are extended to the observing staff at Casey Station, as well as Steve Pendlebury, and Kevin Shepherd (all of BoM), and Neal Young (ACE CRC and AAD). DMSP OLS data were supplied by NOAA. Meteorological data from Dumont d'Urville for 1994 were obtained from the First Regional Observing Study of the (Antarctic) Troposphere, and for 1995 from the British Antarctic Survey (more information available online at http://www.antarctica.ac.uk/met/metlog/). Dome C AWS data were obtained from the Web site of the Antarctic Meteorological Research Center (AMRC), Space Science and Engineering Center, University of Wisconsin—Madison. Macquarie Island data were obtained from BoM. SSM/I ice concentration data were obtained from the NASA Earth Observing System Distributed Active Archive Center (DAAC) at the U.S. National Snow and Ice Data Center, University of Colorado. Data were obtained from ECMWF under the special project ''Assessment of ECMWF forecasts over the high latitude areas of the Southern Hemisphere.'' NNR data were obtained from the NCEP–NCAR reanalysis project at the NOAA–CIRES Climate Diagnostics Center, Boulder, Colorado. Last but not least, we are indebted to Dr. Eric Wolff (British Ant-

arctic Survey) for providing us with his surface observations, and to Will Manning (Raytheon Information Technology and Scientific Services, Maryland), and Robert Gersten (SSAI, Maryland) for processing the SSM/I data.

REFERENCES

Adams, N., 2001: Numerical weather prediction in East Antarctica. Preprints, *Sixth Conf. on Polar Meteorology and Oceanography,* San Diego, CA, Amer. Meteor. Soc., 331–334.

——, 2004: Precipitation forecasting at high latitudes. *Wea. Forecasting,* **19,** 456–472.

Alley, R. B., 1987: Texture of polar firn for remote sensing. *Ann. Glaciol.,* **9,** 1–4.

Allison, I., G. Wendler, and U. Radok, 1993: Climatology of the East Antarctic ice sheet (100°E to 140°E) derived from automatic weather stations. *J. Geophys. Res.,* **98** (D5), 8815–8823.

Bromwich, D. H., 1988: Snowfall in high southern latitudes. *Rev. Geophys.,* **26,** 149–168.

——, 1990: Estimates of Antarctic precipitation. *Nature,* **343,** 627–629.

——, R. I. Cullather, and M. L. Van Woert, 1998: Antarctic precipitation and its contribution to the global sea-level budget. *Ann. Glaciol.,* **27,** 220–226.

Budd, W. F., 1966: Drifting of nonuniform snow particles. *Studies in Antarctic Meteorology,* M. J. Rubin, Ed., AGU Antarctic Research Series, Vol. 9, Amer. Geophys. Union, 59–70.

——, and I. Simmonds, 1991: Impact of global warming on the Antarctic mass balance and global sea level. *Proc. Int. Conf. on the Role of the Polar Regions in Global Change,* Vol. 2, Fairbanks, AK, University of Alaska, Fairbanks, 489–494.

Carleton, A. M., and D. A. Carpenter, 1990: Satellite climatology of ''polar lows'' and broadscale climate associations for the Southern Hemisphere. *Int. J. Climatol.,* **10,** 219–246.

Colbeck, S. C., 1983: Theory of metamorphism of dry snow. *J. Geophys. Res.,* **88** (C9), 5475–5482.

Comiso, J. C., H. J. Zwally, and J. L. Saba, 1982: Radiative transfer modeling of microwave emission and dependence on firn properties. *Ann. Glaciol.,* **3,** 54–58.

Connolley, W. M., and J. C. King, 1993: Atmospheric water vapour transport to Antarctica inferred from radiosondes. *Quart. J. Roy. Meteor. Soc.,* **119,** 325–342.

Cullather, R. I., D. H. Bromwich, and M. L. Van Woert, 1996: Interannual variations in Antarctic precipitation related to El Niño–Southern Oscillation. *J. Geophys. Res.,* **101** (D14), 19 109–19 118.

Delaygue, G., V. Masson, J. Jouzel, R. D. Koster, and R. J. Healy, 2000: The origin of Antarctic precipitation: A modelling approach. *Tellus,* **52B,** 19–36.

Enomoto, H., and Coauthors, 1998: Winter warming over Dome Fuji, East Antarctica and semi-annual oscillation in the atmospheric circulation. *J. Geophys. Res.,* **103** (D18), 23 103–23 111.

Fily, M., and J.-P. Benoist, 1991: Large-scale statistical study of Scanning Multichannel Microwave Radiometer (SMMR) data over Antarctica. *J. Glaciol.,* **37,** 129–139.

Foster, J. L., D. K. Hall, and A. T. C. Chang, 1984: An overview of passive microwave snow research and results. *Rev. Geophys. Space Phys.,* **22,** 195–208.

Fung, A. K., and M. F. Chen, 1981: Emission from an inhomogeneous layer with irregular interfaces. *Radio Sci.,* **16,** 289–298.

——, and H. J. Eom, 1982: Application of a combined rough surface and volume scattering theory to sea ice and snow backscatter. *IEEE Trans. Geosci. Remote Sens.,* **20,** 528–536.

Gibson, T. T., 1995: Atmospheric blocking in the Southern Hemisphere 1982–1992. *Proc. APOC and AMOS Joint Conf.,* Lorne, Australia, Australian Meteorological and Oceanographic Society, 40.

Giovinetto, M. B., and C. R. Bentley, 1985: Surface balance in ice drainage systems of Antarctica. *Antarct. J. U.S.,* **20,** 6–13.

Goodwin, I. D., 1990: Snow accumulation and surface topography in the katabatic zone of eastern Wilkes Land. *Antarct. Sci.,* **2,** 235–242.

——, 1991: Snow-accumulation variability from seasonal observations and firn-core stratigraphy, eastern Wilkes Land, Antarctica. *J. Glaciol.,* **37,** 383–387.

——, M. Higham, I. Allison, and R. Jaiwen, 1994: Accumulation variation in eastern Kemp Land, Antarctica. *Ann. Glaciol.,* **20,** 202–206.

Hirasawa, N., H. Nakamura, and T. Yamanouchi, 2000: Abrupt changes in meteorological conditions observed at an inland Antarctic station in association with wintertime blocking. *Geophys. Res. Lett.,* **27,** 1911–1914.

Kalnay, E., and Coauthors, 1996: The NCEP/NCAR 40-Year Reanalysis Project. *Bull. Amer. Meteor. Soc.,* **77,** 437–471.

Kistler, R., and Coauthors, 2001: The NCEP–NCAR 50-Year Reanalysis: Monthly means CD-ROM and documentation. *Bull. Amer. Meteor. Soc.,* **82,** 247–267.

Lang, R. M., B. R. Leo, and R. L. Brown, 1984: Observations on the growth process and strength characteristics of surface hoar. *Proc. Int. Snow Science Workshop,* Aspen, CO, ISSW Workshop Committee, 188–195.

Legresy, B., and F. Remy, 1997: Antarctic Ice Sheet snow properties derived from ERS altimeter data. *Proc. Third ERS Symp.,* Vol. 2, ESA SP-414, Florence, Italy, European Space Agency, 887–890.

Male, D. H., 1980: Seasonal snow cover. *Dynamics of Snow and Ice Masses,* S. C. Colbeck, Ed., Academic Press, 305–395.

Marques, R. F. C., and V. B. Rao, 1999: A diagnosis of a long-lasting blocking event over the southeast Pacific Ocean. *Mon. Wea. Rev.,* **127,** 1761–1776.

Massom, R. A., M. R. Drinkwater, and C. Haas, 1997: Winter snow cover on sea ice in the Weddell Sea. *J. Geophys. Res.,* **102** (C1), 1101–1117.

——, V. I. Lytle, A. P. Worby, and I. Allison, 1998: Winter snow cover variability on East Antarctic sea ice. *J. Geophys. Res.,* **103** (C11), 24 837–24 855.

Mätzler, C., R. O. Ramseier, and E. Svendsen, 1984: Polarization effects in sea-ice signatures. *IEEE J. Oceanic Eng.,* **9,** 333–338.

McMorrow, A. J., M. A. J. Curran, T. D. van Ommen, V. Morgan, M. J. Pook, and I. Allison, 2001: Intercomparison of firn core and meteorological data. *Antarct. Sci.,* **13,** 329–337.

Mohr, K. I., and E. J. Zipser, 1996: Defining mesoscale convective systems by their ice scattering signature. *Bull. Amer. Meteor. Soc.,* **77,** 1179–1189.

Murray, R. J., and I. Simmonds, 1991: A numerical scheme for tracking cyclone centers from digital data. Part III: Application to January and July general circulation model simulations. *Aust. Meteor. Mag.,* **39,** 167–180.

Noone, D., and I. Simmonds, 1998: Implications for the interpretation of ice-core isotope data from analysis of modelled Antarctic precipitation. *Ann. Glaciol.,* **27,** 398–402.

——, J. Turner, and R. Mulvaney, 1999: Atmospheric signals and characteristics of accumulation in Dronning Maud Land, Antarctica. *J. Geophys. Res.,* **104,** 19 191–19 212.

Palais, J. M., I. M. Whillans, and C. Bull, 1982: Snow stratigraphic studies at Dome C, East Antarctica: An investigation of depositional and diagenetic processes. *Ann. Glaciol.,* **3,** 239–242.

Pettré, P., J. F. Pinglot, M. Pourchet, and L. Reynaud, 1986: Accumulation distribution in Terre Adélie, Antarctica: Effect of meteorological parameters. *J. Glaciol.,* **32,** 486–500.

Pook, M. J., 1995: Atmospheric blocking in the Australasian region in the Southern Hemisphere winter. Ph.D. thesis, University of Tasmania, Hobart, Tasmania, Australia, 168 pp.

——, and L. Cowled, 1999: On the detection of weather systems over the Antarctic interior in the FROST analyses. *Wea. Forecasting,* **14,** 920–929.

——, and T. Gibson, 1999: Atmospheric blocking and storm tracks during SOP-1 of the FROST Project. *Aust. Meteor. Mag.,* June Special Edition, 51–60.

Puri, K., G. S. Dietachmayer, G. A. Mills, N. E. Davidson, R. A. Bowen, and L. W. Logan, 1998: The new BMRC Limited Area Prediction System, LAPS. *Aust. Meteor. Mag.*, **47,** 203–233.

Reid, P. A., and W. F. Budd, 1999: Antarctic circumpolar wave in precipitation and evaporation over the Antarctic continent. WMO Research Activities in Atmosphere and Oceanic Modelling, CAS/JSC Working Group on Numerical Experimentation, World Climate Research Programme Report WMO/TD-942, Dorval, Québec, Canada, 2.31–2.32.

Remy, F., and F. Minster, 1991: A comparison between active and passive microwave measurements of the Antarctic ice sheet and their association with surface katabatic winds. *J. Glaciol.*, **37,** 3–10.

Renwick, J. A., 1998: Variability in the frequency of South Pacific blocking. *Mon. Wea. Rev.*, **126,** 3117–3123.

Schwerdtfeger, W., 1984: *Weather and Climate of the Antarctic*. Vol. 15, *Developments in Atmospheric Science*, Elsevier, 261 pp.

Sherjal, I., and M. Fily, 1994: Temporal variations of microwave brightness temperatures over Antarctica. *Ann. Glaciol.*, **20,** 19–25.

Shuman, C. A., and R. B. Alley, 1993: Spatial and temporal characterization of hoar formation in central Greenland using SSM/I brightness temperatures. *Geophys. Res. Lett.*, **20,** 2643–2646.

——, ——, and S. Anandakrishnan, 1993: Characterization of a hoar-development episode using SSM/I brightness temperatures in the vicinity of GISP2 site, Greenland. *Ann. Glaciol.*, **18,** 195–216.

Sinclair, M. R., 1981: Record high temperatures in Antarctica—A synoptic case study. *Mon. Wea. Rev.*, **109,** 2234–2242.

——, 1994: An objective cyclone climatology for the Southern Hemisphere. *Mon. Wea. Rev.*, **122,** 2239–2256.

——, 1996: A climatology of anticyclones and blocking for the Southern Hemisphere. *Mon. Wea. Rev.*, **124,** 245–263.

Smith, I. N., W. F. Budd, and P. A. Reid, 1998: Model estimates of Antarctic accumulation rates and their relationship to temperature changes. *Ann. Glaciol.*, **27,** 246–250.

St. Germain, K. M., 1994: A two-phase algorithm to correct for atmospheric effects on the 85 GHz channels of the SSM/I in the Arctic regions. *Proc. Int. Geoscience and Remote Sensing Symp.*, Vol. 1, Pasadena, CA, IEEE, 67–69.

Surdyk, S., and M. Fily, 1995: Results of a stratified snow emissivity model based on the wave approach: Application to the Antarctic Ice Sheet. *J. Geophys. Res.*, **100** (C5), 8837–8848.

Trenberth, K. E., and K. C. Mo, 1985: Blocking in the Southern Hemisphere. *Mon. Wea. Rev.*, **113,** 3–21.

Turner, J., and M. Row, 1995: Polar phenomena. *Images in Weather Forecasting*, M. J. Bader et al., Eds., Cambridge University Press, 484–490.

——, W. M. Connolley, S. Leonard, G. J. Marshall, and D. G. Vaughan, 1999: Spatial and temporal variability of net snow accumulation over the Antarctic from ECMWF reanalysis project data. *Int. J. Climatol.*, **19,** 697–724.

——, S. A. Harangozo, G. J. Marshall, J. C. King, and S. R. Colwell, 2002: Anomalous atmospheric circulation over the Weddell Sea, Antarctica during the austral summer of 2001/02 resulting in extreme sea ice conditions. *Geophys. Res. Lett.*, **29,** 2160, doi: 10.1029/2002GL015565.

Ulaby, F. T., R. K. Moore, and A. K. Fung, 1981: Microwave remote sensing fundamentals and radiometry. *Microwave Remote Sensing*, D. S. Simonett, Ed., Artech House, 210–217.

van Lipzig, N. P. M., E. van Meijgaard, and J. Oerlemans, 2002: The spatial and temporal variability of the surface mass balance in Antarctica: Results from a regional atmospheric climate model. *Int. J. Climatol.*, **22,** 1197–1217.

Vaughan, D. G., J. L. Bamber, M. Giovinetto, J. Russell, and A. P. R. Cooper, 1999: Reassessment of surface mass balance in Antarctica. *J. Climate*, **12,** 933–946.

Warren, S. G., 1996: Antarctica. *Encyclopedia of Climate and Weather*, S. H. Schneider, Ed., Vol. 1, Oxford University Press, 32–39.

Wendler, G., and Y. Kodama, 1984: On the climate of Dome C, Antarctica, in relation to its geographical setting. *J. Climatol.*, **4,** 495–508.

Wentz, F. J., 1991: User's manual SSM/I antenna temperature tapes, revision 1. Remote Sensing Systems Tech. Rep. 120191, Santa Rosa, CA, 70 pp.

White, W. B., and R. G. Peterson, 1996: Antarctic circumpolar wave in surface pressure, wind, temperature and sea-ice extent. *Nature*, **380,** 699–702.

Wright, A. D. F., 1974: Blocking action in the Australian region. Australian Bureau of Meteorology Tech. Rep. 10, Melbourne, Australia, 29 pp.

Xie, Z. C., J. Li, and N. W. Young, 1989: Physical characteristics of the snow and ice cover of Law Dome, East Antarctica. *Proceedings of the International Symposium on Antarctic Research*, G. Kun, Ed., China Ocean Press, 8–22.

Zwally, H. J., 1977: Microwave emissivity and accumulation rate of polar firn. *J. Glaciol.*, **18,** 195–215.

——, and M. B. Giovinetto, 1995: Accumulation in Antarctica and Greenland derived from passive-microwave data: A comparison with contoured compilations. *Ann. Glaciol.*, **21,** 123–130.

——, and Coauthors, 2002: ICESat's laser measurements of polar ice, atmosphere, ocean, and land. *J. Geodyn.*, **34,** 405–445.